THE JOURNAL OF PHYSICAL CHEMISTRY C
A JOURNAL OF THE AMERICAN CHEMICAL SOCIETY

pubs.acs.org/JPCC
Article

Machine Learning-Based Interpretation of Optical Properties of Colloidal Gold with Convolutional Neural Networks

Frida Bilén, Pernilla Ekborg-Tanner, Antoine Balzano, Michaël Ughetto, Robson Rosa da Silva, Hannes Schomaker, Paul Erhart, Kasper Moth-Poulsen, and Romain Bordes*

Cite This: https://doi.org/10.1021/acs.jpcc.4c02971
Read Online

ABSTRACT: Gold nanoparticles are used in a range of applications, but their properties depend on their shape, size, and polydispersity. A quick, easy, and accurate characterization of the particles is therefore of high importance, especially in flow synthesis settings where continuous monitoring of the characteristics is desired. Our hypothesis was that convolutional neural networks can be used to extract detailed information about structural parameters of gold nanoparticles from their UV−vis spectra, and we have shown that this is possible by predicting size distributions from *in silico* UV−vis spectra for colloidal gold with high accuracy. Here this was done for both spherical and rod-shaped gold nanoparticles. We also show that the addition of noise makes the prediction of diameter polydispersity more challenging, but the average diameter, and for rods also aspect ratio distribution, can be accurately predicted even with the highest evaluated level of noise. The model structure is promising and worthy of implementation to enable predictions beyond *in silico* generated spectra. The model, for instance, can find application in flow synthesis settings to create a machine learning-driven feedback loop for automated synthesis.

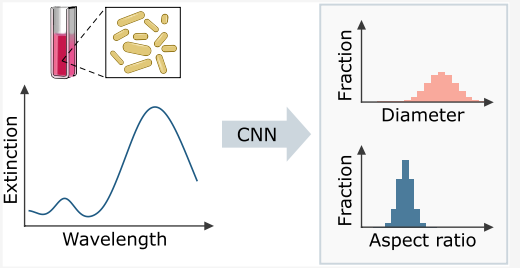

INTRODUCTION

Gold nanoparticles (AuNPs) find use in many different fields ranging from catalysis[1,2] to biological applications such as biosensing,[1,3] photothermal cancer therapy,[2−4] and disease diagnostics.[1−3] Many of the properties central to these applications relate directly to the shape and size of the particles along with their polydispersity,[4−6] and it is therefore crucial to control and characterize these parameters.

In many cases, it is desirable to have a fast and automated characterization of the particle characteristics. This is especially important in flow synthesis settings, where it is optimal with an inline characterization of the particles to determine their sizes and shapes in real time. However, the techniques used today are often expensive, time-consuming, and not compatible with flow synthesis systems. The most common technique for the determination of the nanoparticle structural features, i.e. size, shape, and size distribution, is electron microscopy.[1,7−9] While electron microscopy techniques such as transmission electron microscopy (TEM) give detailed information about both the shape and size of the particles, the technique is time-consuming[8,9] and only a small fraction of the particles can be studied at a time, meaning it might not be representative for the whole sample.[7,9] There are however other techniques used for the determination of AuNP morphology. Small-angle X-ray scattering (SAXS) is one example that studies a bulk section of the sample[7] and can be connected in line with a flow synthesis setup.[9] However, challenges with SAXS include long times for data acquisition,[9] radiation-induced damage to the sample,[9] and that synchrotron X-ray sources are needed for high-resolution SAXS.[4] Dynamic light scattering (DLS), another bulk-scale characterization technique,[7] also comes with drawbacks, as DLS measures the hydrodynamic size and can overestimate the size or polydispersity, especially for non-spherical particles or polydisperse mixtures.[10,11] Beyond that, both techniques are restricted to the investigation of very simple nanocrystal geometries. There are other techniques used for AuNP characterization, such as inductively coupled plasma mass spectrometry (ICP-MS),[12,13] atomic force microscopy (AFM)[1] and X-ray diffraction,[1] but in this paper, we will focus on one technique that fulfills the requirement of being both quick, cheap and with inline capabilities: Ultraviolet−visible (UV−vis) spectroscopy.

UV−vis spectroscopy can be exploited to gain relevant insights of nanoparticle structure since the localized surface plasmon resonance (LSPR) bands of noble metal nanoparticles correlate with their shape, size, and composition.[1,6] Absorption spectrophotometers can be easily coupled to flow chemistry,[14] and provide quick measurements of the absorption and scattering of a sample, with little sample preparation and

Received: May 6, 2024
Revised: July 12, 2024
Accepted: July 30, 2024

without altering the sample.[8] Although the optical properties are correlated to the size and shape of the particles, it can be challenging to extract this information from the spectrum. Some trends can be determined visually as, for example, the shape and size of the particles can affect the number of LSPR bands in the spectrum,[6] and the wavelength of the surface plasmon band maximum (λ_{SPR}) is related to the average diameter of gold nanospheres[1,6] and linearly proportional to the aspect ratio for rod-shaped particles.[2] There are several examples where such parameters in the spectrum, e.g., absorption maximum, the full width at half-maximum (FWHM), or wavelength of the LSPR band, have been used for the determination of AuNP sizes.[15−19] Most of these are however only useful for the determination of the average size of monodisperse samples, and not for finding the size distribution. Another approach for the determination of the nanoparticle characteristics is by fitting of the UV−vis spectrum using models based on, e.g., Mie theory or extensions thereof. This has been used in several studies to predict the average sizes or size distribution of gold nanoparticles from their UV−vis spectra.[8,11,20−22]

Another methodology with the potential to interpret particle properties from spectra is machine learning (ML). An ML model can determine information about a sample without the need to understand the underlying phenomena, i.e., without any information about, e.g., surface plasmon resonance when it comes to AuNPs. Various types of ML algorithms have been applied to spectroscopy before,[23] and ML has been used previously to assist the synthesis of various nanoparticles,[24] for example, by predicting the outcome from a reaction based on the synthesis conditions, or for experiment planning where the model suggests the following steps. ML has also been used previously for characterization in combination with spectroscopy applied to nanomaterials, which is of particular relevance for plasmonic nanoparticles. For example, ML has been used to characterize or design nanoparticles and other nanomaterials from given spectroscopic data.[25−33] This has been done, for example, to find a suitable nanoparticle design that gives desired optical properties,[27,29−31] or to determine nanoparticle shape or size directly from their spectra or from descriptors such as λ_{SPR} and FWHM.[25,28,29,32,33]

One machine learning algorithm that is of particular interest for array-like data such as spectra or images, is convolutional neural network (CNN) architectures. CNNs can handle complex datatypes such as images or spectra as input, which often minimizes the need for dimensionality reduction and preprocessing.[23,34] This also means it can utilize the full spectrum as input. CNN models can find patterns within adjacent data points by processing the input with different so-called kernels that recognize various patterns in the data. By stacking several convolutional layers, more and more complicated shapes can be identified. CNNs are often applied to supervised machine learning, which means it is trained on data pairs consisting of an input with its designated label.[34] The model is then trained to predict the label based on the input. For this application, the input could be a spectrum, and the label some information about the sample, for example, the particle size. A challenge with the data-driven machine learning approach is the large amount of these data pairs that are needed for the training, which can be time-consuming to generate experimentally.

CNNs have been used for the interpretation of spectra before.[23] For example, He et al. used a bidirectional neural network model with a CNN part to determine the size parameters of gold nanospheres, nanorods, and dimers from given absorption, scattering, and extinction spectra.[29] We hypothesize that machine learning, and in particular CNNs, can extract more detailed structural information about AuNPs, such as polydispersity, directly from UV−vis spectra.

In this paper, we use convolutional neural network models to determine both the average size and polydispersity of gold nanoparticles from simulated UV−vis spectra. Spherical and rod-shaped particles are studied to represent particle shapes with one and two parameters for the size, respectively. The training and testing were done on *in silico* data as a first step, due to the large amounts of data required for the model training. We also tested the robustness of the models against noise, as a first step toward predictions based on experimental data.

METHODS

Simulations of Single Particle Spectra with the Finite-Difference Time-Domain Method. The single particle spectra were simulated using the MEEP software,[35] which implement the finite-difference time-domain (FDTD) method to evolve the Maxwell equations in time on a grid where the materials properties are varied to simulate, e.g., a nanoparticle in a dielectric environment. FDTD methods are widely used in the field of computational electromagnetics due to their flexibility, simplicity, and stability for many problems.[36,37] The benefits of FDTD include that no approximations to the governing Maxwell equations are needed and entire extinction spectra can be calculated via a single simulation.

The computational cell consists of a gold nanosphere or nanorod in water. Gold is represented by a dielectric function from the MEEP library and water by a constant refractive index of 1.333. The nanorods are characterized by their diameter and aspect ratio (AR), where AR = 1 corresponds to a nanosphere. In the present work, diameters between 10 and 100 nm (with a step size of 2 nm) and AR between 1 to 4 (with a step size of 0.25) are considered. To mimic an infinite system, the computational cell is enclosed by a 100 nm thick perfectly matched layer (PML) placed such that the distance to the nanoparticle is at least 100 nm in all directions. The source is a Gaussian pulse corresponding to the energy interval 1−4 eV propagating in the direction perpendicular to the rod axis and polarized at 45° from the rod axis. The grid is Cartesian with a resolution of 0.6 pixels/nm.

The simulations begin with the incoming Gaussian pulse exciting the system and end when the amplitude of the electric field has decayed by a factor of 10^{-6} compared to its previous maximum value. To calculate the extinction spectra, two simulations are performed. The first simulation is carried out without the nanoparticle to obtain the incoming intensity and fluxes for normalization purposes. In the second simulation, the power transmitted through a closed surface surrounding the nanoparticle is calculated by integrating the Poynting vector and normalized by the incoming intensity to obtain the absorption cross section. The scattering cross section is obtained in similar fashion, with the difference that fluxes from the first simulation are subtracted before calculating the transmitted power through the same surface in the outward direction, as opposed to the inward direction for the absorption. Lastly, the extinction is obtained as the sum of absorption and scattering.

https://doi.org/10.1021/acs.jpcc.4c02971
J. Phys. Chem. C XXXX, XXX, XXX−XXX

A visual examination of the single particle spectra was made, to identify the need for preprocessing of the data. A few spectra that were diverging from the expected patterns were identified, and these were replaced by interpolations, typically of the spectra with the same AR but 2 nm larger and 2 nm smaller diameter. Additional preprocessing was made by limiting the wavelengths to 400−800 nm for the nanospheres and 400−1000 nm for the nanorods, as rod-shaped particles typically have more extinction at longer wavelengths compared to spherical particles with similar diameters.

Generation of Spectra for Polydisperse Systems. For the spherical systems, the mean and standard deviation of a Gaussian distribution were randomized for each sample, where the mean (a random number in the interval [30, 80) nm) represents the average diameter and the standard deviation (a random number in the interval [1, 8) nm) represents the polydispersity. For the rods, the diameter distribution was chosen in the same way as for the spheres, and the AR distribution was chosen with a mean in the interval [2, 3.5), and standard deviation in the interval [0.3, 1).

To create each polydisperse spectrum, 100,000 instances were drawn from the given distribution, where each instance represents a specific nanoparticle size. The single particle spectra of these 100,000 instances were then added together to create an *in silico* mixing of particles of different sizes and generate the additive spectrum of this mixture. Thus, the additive spectrum represents a dilute suspension of polydisperse gold nanoparticles in water, not considering interactions between the particles such as plasmon coupling. Min-max scaling was applied to the spectra, to have the extinction between 0 and 1 for all samples. Data sets of 1500 and 3000 spectra were constructed for the sphere and rod models, respectively.

For the spectra with added noise, the same process was followed, and then the noise was added to the spectra. To each data point in each spectrum, the added noise was from a normal distribution with mean 0 and standard deviations of 0.0025, 0.0050, 0.0100, 0.0200, or 0.0300, where a larger standard deviation gives a noisier spectrum. The spectra were then min-max scaled again to have the extinction between 0 and 1.

Construction of the CNN Model. The models used for the prediction tasks were constructed using Keras[38] (version 2.5.0) as the deep learning framework and Python (version 3.8.3) as the programming language. The models were trained to take the simulated polydisperse spectra as input and predict the means and standard deviations of the Gaussian size distributions used for the generation of the spectra.

The full architectures of the convolutional neural network models are presented in the Supporting Information. The input layer is composed of one node for each data point in the input spectroscopic data. This is then followed by four convolutional layers in total, two max pooling layers and two fully connected layers, according to Table 1. The 2D versions of the convolutional and max pooling layers are chosen to enable compatibility with other functionalities that are out of scope for this work, but in principle, they act as 1D layers as the size of the first dimensionality is 1. The output layer has 2 and 4 nodes for the sphere and rod models respectively, representing the descriptors of the size distribution (mean and standard deviation of the diameter distribution for spheres, and diameter and aspect ratio distributions for rods). ReLU was used as the activation function for the convolutional layers and the first fully connected (dense) layer, while the second dense layer (the output layer) had no activation function. The model architecture and hyperparameters of the models were tuned to give satisfactory results while preventing excessive training times for the model, where the performance was evaluated in terms of the mean squared error (MSE) and the coefficient of determination (R^2) scores for the predicted versus true size parameters.

Table 1. Model Architecture for the Two Models

layer[a]	parameters for the sphere model	parameters for the rod model
Conv2D	8 (1,150)	16 (1,50)
Conv2D	16 (1,120)	32 (1,40)
MaxPooling2D	(1,2), (1,2)	(1,2), (1,2)
Conv2D	32 (1,80)	64 (1,20)
Conv2D	64 (1,40)	128 (1,10)
MaxPooling2D	(1,2), (1,2)	(1,2), (1,2)
Dense	30	60
Dense	2	4

[a]For the convolutional layers, the number of filters and (kernel size) are presented. All max pooling layers have the pool size (1,2) and strides (1,2). For the fully connected (dense) layers the number of neurons is presented.

The training and testing of the models were done with data sets of 1500 and 3000 samples for the sphere and rod models respectively, where 30% of the data was used for the test set and 70% for the training. Out of the training data set, 30% was used for validation during the training. Adam was used as the optimization algorithm with a learning rate of 0.001 and MSE was used as the loss function for the assessment of the model performance. The training was done for 600 epochs with the ModelCheckpoint callback function to load the weights from the best epoch, and a batch size of 100 was used. Three replicates with different TensorFlow random seeds were made for each level of noise on the data.

RESULTS AND DISCUSSION

Simulations and Generation of *In Silico* Data. Spectra for single gold nanoparticles of different sizes were simulated using the finite-difference time-domain (FDTD) method. A small portion of these spectra suffered from numerical instabilities and were replaced by interpolations based on the other spectra (see Figures S1−S3 in Supporting Information for details). The wavelengths were also limited to avoid unwanted discrepancies that were present at wavelengths above 1000 nm. Examples of the single particle spectra, with and without preprocessing, can be found in Figures S1−S3 in the Supporting Information.

To mimic spectra for polydisperse mixtures of AuNPs, weighted sums of the single particle spectra were taken according to Gaussian size distributions with randomized means and standard deviations. For spherical particles, one size distribution was specified for each sample, where the mean represents the average diameter, and the standard deviation represents the polydispersity of diameters in the sample. For the rod-shaped particles, the same was done but with two distributions, representing the diameter distribution and the aspect ratio (AR) distribution, respectively. For some experiments, artificial noise was added to the spectra to simulate the disturbances that are usually present in experimentally gathered spectra. Examples of the *in silico* generated spectra

https://doi.org/10.1021/acs.jpcc.4c02971
J. Phys. Chem. C XXXX, XXX, XXX−XXX

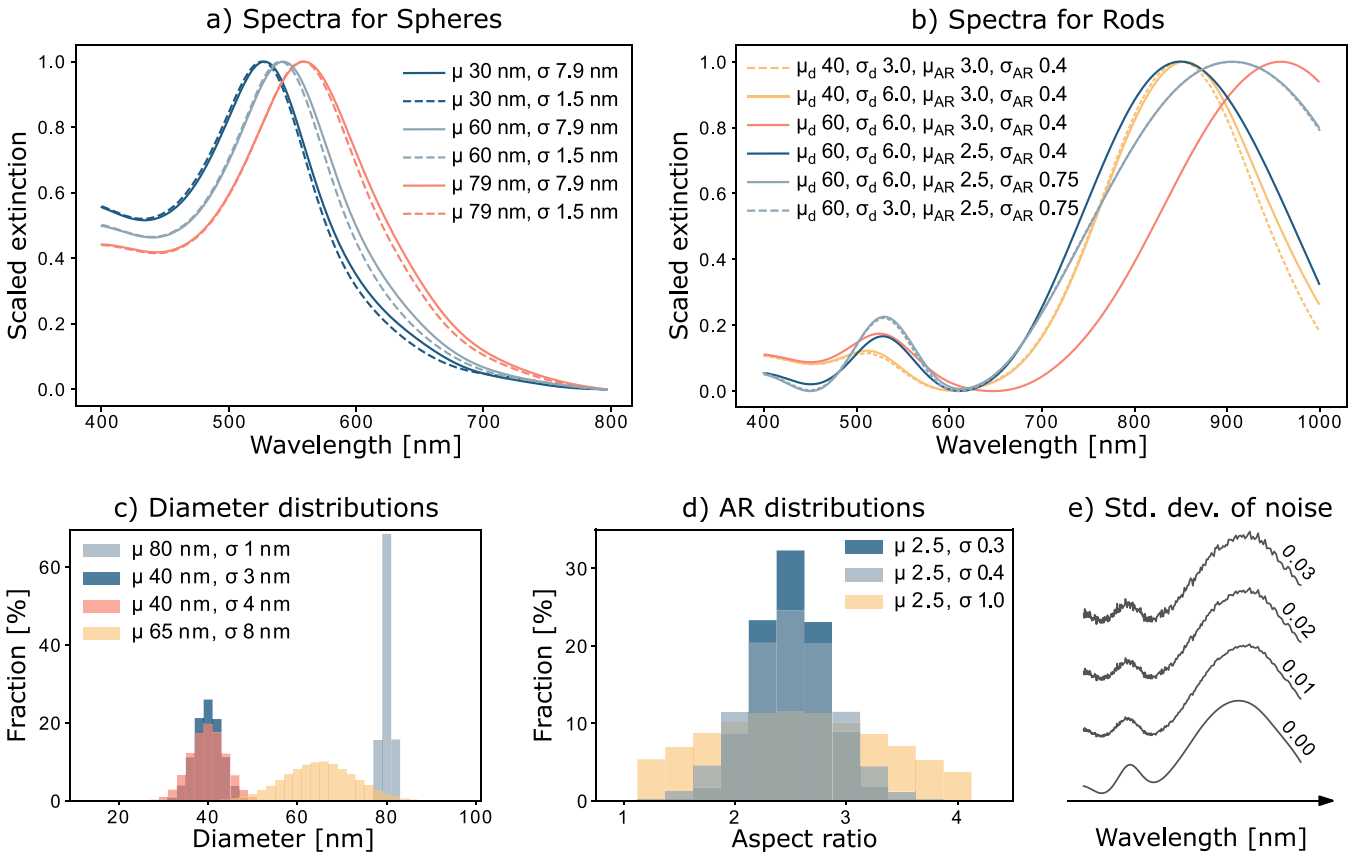

Figure 1. Examples of simulated data. At the top: simulated spectra for polydisperse mixtures of nanoparticles, spherical particles to the left (a) and rod-shaped particles to the right (b). At the bottom: examples of diameter distributions to the left (c), examples of aspect ratio distributions in the middle (d), and examples of a spectrum with varying levels of added noise (expressed as the standard deviation of the normal distributed noise) to the right (e). The mean of a distribution is denoted as μ and the standard deviation as σ.

with different size distributions for spherical and rod-shaped particles, examples of diameter- and AR distributions, and examples of spectra with varying levels of noise are presented in Figure 1.

In Figure 1, it can be seen that for spherical particles the mean of the diameter distribution (i.e., the average size) has a larger effect on the spectrum compared to the standard deviation (the polydispersity). An increased average size increases the wavelength of the extinction maximum, while only minor changes can be seen when the polydispersity is varied. For rod-shaped particles, a similar trend is seen, where a change in the polydispersity of diameters only gives small variations in the spectrum (compare dashed and solid lines). The other size distribution parameters (average diameter, average AR, and polydispersity of AR) give larger variations, although it can be seen that different combinations of parameters can result in similar spectral response, see for example the comparison between the yellow solid line (μ_d = 40 nm, σ_d = 6.0 nm, μ_{AR} = 3.0, σ_{AR} = 0.4) and blue solid line (μ_d = 60 nm, σ_d = 6.0 nm, μ_{AR} = 2.5, σ_{AR} = 0.4), which have completely different size distributions but similar wavelengths for maximum extinction. This illustrates the challenge with manual determination of size distributions from spectra. The data sets with polydisperse spectra are available for download at https://git.chalmers.se/projects/15792.

The data sets with spectra for polydisperse mixtures and their respective size distributions were divided into two groups, where one was used for the training and validation of the model, and the other for testing its performance.

Predictions of Size Distributions (No Noise). Two convolutional neural network models were set up, one model for spheres and one for rods. The models were constructed to take a spectrum as input and predict the size distribution parameters that were used to generate the spectrum for the polydisperse mixture. Various model structures with different parameters were evaluated, and the final model structures that performed well without excessive training times were constructed with in total four convolutional layers, two max pooling layers and two fully connected layers. Both models are available at https://git.chalmers.se/projects/15792. The performance was evaluated in terms of the mean squared error and the coefficients of determination (R^2) for the predicted versus true size parameters.

After the training of the models, they were tested on data sets with spectra not previously seen by the model.

Case 1: Spheres. For each spectrum in the test set, the model for spherical particles predicted the average diameter and polydispersity of the particle mixture, represented by the mean and standard deviation of a Gaussian size distribution. The results from this test set are presented in Figure 2a,b, where each data point represents one sample in the test set. As can be seen in these figures, the model can accurately predict both the average diameter and the polydispersity of the particle mixture, with an R^2 of 0.9993 and 0.9764, respectively. Figure 2c shows one representative example of the predicted size

https://doi.org/10.1021/acs.jpcc.4c02971
J. Phys. Chem. C XXXX, XXX, XXX−XXX

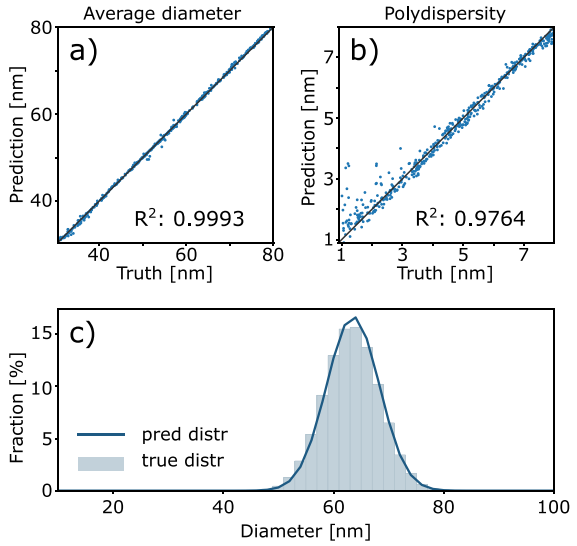

Figure 2. Predicted vs true parameters for the size distributions of all spectra in the test data set for spheres, for the average diameter in (a) and standard deviation of the distribution in (b). (c) shows one representative example of the predicted and true distribution for one of the spectra.

distribution compared to the true size distribution used for the generation of the spectrum of that specific sample.

For the narrowest size distributions, i.e., polydispersity values below 3 nm, the model overestimates the polydispersity in a few instances in the test set. No trend could be seen regarding the average diameters of these instances, however. Overall, when considering the small differences displayed by the spectra for different polydispersities, see dashed compared to solid lines in Figure 1a, the CNN could discriminate and predict accurately both average size and polydispersity from a single UV−vis spectrum.

Case 2: Rod-Shaped Particles. In order to adapt the CNN to a four-parameter system (diameter, AR and their related polydispersities), adjustments were done in terms of nodes in the output layer, but also number of filters and kernel sizes in the convolutional layers, and number of hidden units in the fully connected layer. More filters but of a smaller kernel size appeared to improve the predictions for the rods, compared to the model structure used for the spheres.

The model for rod-shaped nanoparticles can accurately predict the parameters of the size distributions from UV−vis spectra, see Figure 3a-d, where each data point represents one sample in the test set and the diagonals show where the predicted and true values are the same. The results are especially accurate for the average diameter (Figure 3a), average aspect ratio (Figure 3c), and polydispersity of the aspect ratio (Figure 3d), for which the R^2 is above 0.99. The performance for the prediction of the polydispersity of the rod diameters is slightly lower (R^2 of 0.8497), but this was expected considering that changes in this parameter only have very minor effects on the spectral response, as can be seen when comparing dashed and solid lines of the same color in Figure 1b. These results are still accurate, however, and less than 18% of the samples in the test set have an error in diameter polydispersity larger than 1 nm. Examples of diameter distributions can be seen in Figure 1c, where the dark blue and red distributions have a 1 nm difference in polydispersity. Representative examples of the predicted and true distributions of the rod diameter and aspect ratio are presented in Figure 3e,f respectively.

The results from the tests with simulated data without added noise show that the CNN models for both particle shapes can interpret the information from the simulated UV−vis spectra and accurately predict the size distributions of the particles. For both particle shapes, it could be seen that the polydispersity of the diameter was the most challenging prediction task, with a slightly lower R^2 than for the other parameters.

Effect of Noise. As a first step toward the use of the models in an experimental setting, it was desired to test the robustness of the models when the data has a closer resemblance to real

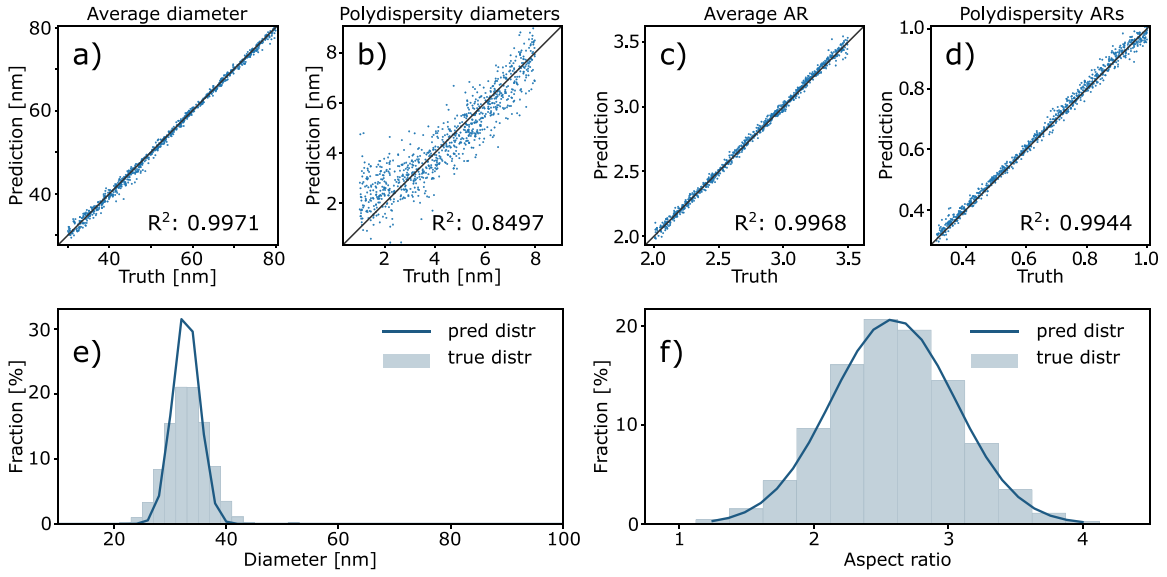

Figure 3. Results from the predictions on the test set for the rods. (a−d) Predicted vs true parameters for the size distributions: average diameter, standard deviation of the diameter distribution, average AR and standard deviation of the AR distribution respectively. One representative example of the predicted and true size distribution can be seen in (e) and (f), for the distribution of diameters and ARs respectively.

https://doi.org/10.1021/acs.jpcc.4c02971
J. Phys. Chem. C XXXX, XXX, XXX−XXX

spectroscopic data. Therefore, to bridge the gap between the smooth simulated spectra and more complex experimental ones, tests were also made with spectra that had different levels of noise. The noise was created by the addition of random numbers from a normal distribution centered on 0 to all data points in the spectrum, and the level of noise was defined as the standard deviation of the distribution, see Figure 1 for examples.

Case 1: Spheres. When the model was trained and tested on data with added noise, it can still very accurately predict the average diameter, even with the highest amount of noise added in this work, see Figure 4. This indicates that the model is

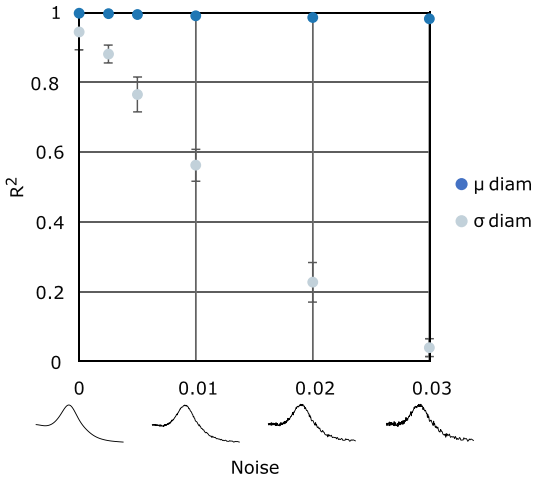

Figure 4. Effect on prediction performance of different noise levels added to the spectra, visualized as the coefficient of determination (R^2) as a function of the standard deviation of the normal distributed noise. μ represents the mean of the size distribution, and σ the standard deviation. The error bars show the standard deviation of the results from three replicates.

robust also for finding the average sizes of AuNPs in experimental data. The prediction of the polydispersity was, however, more challenging, and the performance rapidly decreases upon the addition of increasing levels of noise. This could be explained by the very subtle differences between spectra with different polydispersities (see Figure 1a), which are smeared by the addition of noise, making the prediction task very challenging. For experimental spectra recorded under appropriate conditions on high-quality spectrophotometers, the noise levels are typically low, see examples in Supporting Information Figure S4, at which the model can still predict the polydispersity well. These results however indicate that spectra with more noise, for example, spectra collected with a short acquisition time in an inline setting, might require some denoising before the prediction is done to improve the quality of the prediction.

Case 2: Rod-Shaped Particles. As for the prediction on spectra for spherical particles, the model for rod-shaped particles was sensitive against noise when it comes to the prediction of diameter polydispersity. Even with small levels of noise, the performance decreased quite drastically for this prediction, see Figure 5. Again, this could be explained by the minute changes observed upon variations in the diameter polydispersity, and that these small differences are likely lost when the noise is added. As discussed for the spherical particles, this could indicate that for future application of the

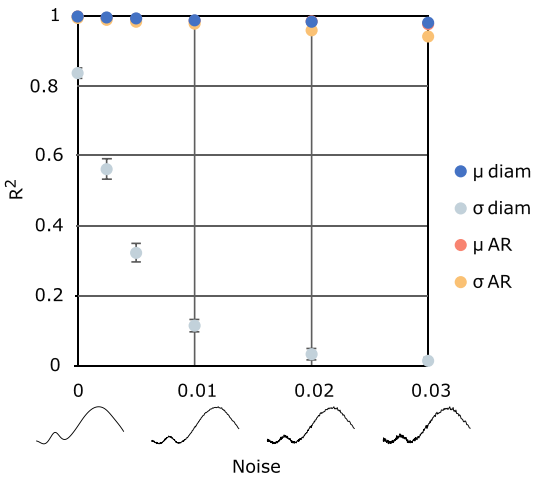

Figure 5. Effect on prediction performance of different noise levels added to the spectra, visualized as the coefficient of determination (R^2) as a function of the standard deviation of the normal distributed noise. μ represents the mean of the size distribution, and σ the standard deviation. The error bars show the standard deviation of the results from three replicates.

model to experimental data, a noise reduction on the spectra could be beneficial to improve the accuracy of the diameter polydispersity prediction. The predictions of the other parameters, however, seemed to be robust against noise, and the R^2 scores for these predictions were above 0.9 even for the highest level of noise in the tests.

CONCLUSIONS

Inline data analysis in continuous flow synthesis is a cornerstone for complete automation of gold nanoparticle synthesis. UV−vis spectroscopy is a well-suited inline characterization of AuNPs, as the extinction bands are related to the shape and size of the nanoparticles due to the localized surface plasmon resonance. It is however challenging to interpret the particle characteristics from the spectra, especially for polydisperse mixtures of particles.

In this study, we tested if CNNs can be used to extract detailed information about structural parameters of gold nanoparticles from their UV−vis spectra. CNNs have previously been used to predict average sizes of gold nanoparticles,[29] but we have shown that it is possible to predict even more complex information by predicting the average size and polydispersity of size distributions for colloidal gold from *in silico* UV−vis spectra with high accuracy. Here this was done for both spherical and rod-shaped gold nanoparticles, where the model for spheres predict the average diameter and standard deviation of a Gaussian size distribution with coefficients of determination (R^2) of 0.9993 and 0.9764, respectively, and the model for rod-shaped particles predicts the mean and standard deviation for both the distribution of diameters and aspect ratios, with an R^2 of 0.8497 for the standard deviation of the rod diameters, and above 0.99 for the other parameters. These results show that the models used, with in total four convolutional layers, two max pooling layers, and two fully connected layers, are sufficient to predict these parameters for the simulated, noise-free data.

As a first step toward the intended application, i.e., using the models in an experimental flow synthesis setting, the models were trained and tested on data with added noise. The addition

https://doi.org/10.1021/acs.jpcc.4c02971
J. Phys. Chem. C XXXX, XXX, XXX−XXX

of noise makes the prediction of diameter polydispersity more challenging, and the R^2 for this parameter decreases rapidly with the standard deviation of the noise for both the spherical and rod-shaped particles. The reason for this is likely the very subtle differences in the spectrum as the diameter polydispersity is changed, which gets lost as the noise is added. This could be an indication of potential challenges when applying the models to experimental data, which naturally has some level of noise. One potential remedy to the decrease in performance for data with this kind of disturbances could be to not only train the model on noisy data but to also do noise reduction on the experimental spectra before the prediction is initiated. For the other predicted parameters, however, i.e., the average diameter and the distribution of aspect ratios for the rods, the predicted values are still very accurate with R^2s above 0.9 even for the highest level of noise that was used in the evaluations.

The results for the noise free simulated data show that the model structure is promising, but the fact that the *in silico* data is diverging significantly from experimental data and the challenges faced from the predictions on noisy spectra, show that training of the model should also be done on experimental spectra of gold nanoparticle mixtures. The divergence from experimental data is likely due to, e.g., not accounting for capping agents or plasmon coupling in the simulations or limitations of the *in silico* mixing. To mitigate the consequences of smaller data sets, transfer learning[39] might be used in a way so that the current training is utilized as a base, and the additional training requires less data.

■ ASSOCIATED CONTENT

Supporting Information

The Supporting Information is available free of charge at https://pubs.acs.org/doi/10.1021/acs.jpcc.4c02971.

Visualization of simulated single particle spectra, with preprocessing examples; model architectures; experimental spectra for comparisons (PDF)

■ AUTHOR INFORMATION

Corresponding Author

Romain Bordes − *Department of Chemistry and Chemical Engineering, Chalmers University of Technology, Gothenburg 412 58, Sweden;* orcid.org/0000-0002-0785-2017; Email: bordes@chalmers.se

Authors

Frida Bilén − *Department of Chemistry and Chemical Engineering, Chalmers University of Technology, Gothenburg 412 58, Sweden;* orcid.org/0000-0003-1130-2429

Pernilla Ekborg-Tanner − *Department of Physics, Chalmers University of Technology, Gothenburg 412 96, Sweden;* orcid.org/0000-0002-9427-4816

Antoine Balzano − *Department of Chemistry and Chemical Engineering, Chalmers University of Technology, Gothenburg 412 58, Sweden*

Michaël Ughetto − *BIKG, AI Strategy & Innovation, R&D IT, Mölndal 431 83, Sweden*

Robson Rosa da Silva − *Department of Chemistry and Chemical Engineering, Chalmers University of Technology, Gothenburg 412 58, Sweden; NanoScientifica Scandinavia AB, Gothenburg 412 96, Sweden;* Present Address: Robson Rosa da Silva present address: NanoScientifica Scandinavia AB, Gothenburg, 412 96, Sweden (R.R.D.S.); orcid.org/0000-0001-6887-4749

Hannes Schomaker − *Department of Chemistry and Chemical Engineering, Chalmers University of Technology, Gothenburg 412 58, Sweden; AutoSyn AB, Hisings Backa 422 57, Sweden;* Present Address: Hannes Schomaker present address: AutoSyn AB, Hisings Backa, 422 57, Sweden (H.S.).

Paul Erhart − *Department of Physics, Chalmers University of Technology, Gothenburg 412 96, Sweden;* orcid.org/0000-0002-2516-6061

Kasper Moth-Poulsen − *Department of Chemistry and Chemical Engineering, Chalmers University of Technology, Gothenburg 412 58, Sweden; Department of Chemical Engineering, Universitat Politècnica de Catalunya, Barcelona 08019, Spain; Catalan Institution for Research & Advanced Studies, ICREA, Barcelona 08010, Spain; Institute of Materials Science of Barcelona, ICMAB-CSIC, Barcelona 08193, Spain;* orcid.org/0000-0003-4018-4927

Complete contact information is available at: https://pubs.acs.org/10.1021/acs.jpcc.4c02971

Author Contributions

F.B. performed conceptualization, writing−original draft, writing−review and editing, and investigation. P.E.-T. performed conceptualization, writing−original draft, writing−review and editing, and investigation. A.B. performed investigation. M.U. performed supervision. R.R.d.S. performed conceptualization and writing−review and editing. H.S. performed conceptualization and writing−review and editing. P.E. performed conceptualization, supervision, and writing−review and editing. K.M.-P. performed conceptualization and writing−review and editing. R.B. performed conceptualization, supervision, and writing−review and editing.

Funding

The authors are grateful for the financial support from the Swedish Research Council (VR) and the Excellence Initiative Nano at Chalmers. The electromagnetic simulations were enabled by resources provided by the National Academic Infrastructure for Supercomputing in Sweden (NAISS) at C3SE.

Notes

The authors declare no competing financial interest.

■ ABBREVIATIONS

AuNPs, gold nanoparticles; TEM, transmission electron microscopy; SAXS, small-angle X-ray scattering; DLS, dynamic light scattering; LSPR, localized surface plasmon resonance; FWHM, full width at half-maximum; ML, machine learning; CNN, convolutional neural network; FDTD, finite-difference time-domain; PML, perfectly matched layer; MSE, mean squared error; AR, aspect ratio

■ REFERENCES

(1) Daniel, M.-C.; Astruc, D. Gold Nanoparticles: Assembly, Supramolecular Chemistry, Quantum-Size-Related Properties, and Applications toward Biology, Catalysis, and Nanotechnology. *Chem. Rev.* **2004**, *104* (1), 293−346.

(2) Huang, X.; Neretina, S.; El-Sayed, M. A. Gold Nanorods: From Synthesis and Properties to Biological and Biomedical Applications. *Adv. Mater.* **2009**, *21* (48), 4880−4910.

(3) Dreaden, E. C.; Alkilany, A. M.; Huang, X.; Murphy, C. J.; El-Sayed, M. A. The golden age: gold nanoparticles for biomedicine. *Chem. Soc. Rev.* **2012**, *41* (7), 2740−2779.
(4) Lohse, S. E.; Murphy, C. J. The Quest for Shape Control: A History of Gold Nanorod Synthesis. *Chem. Mater.* **2013**, *25* (8), 1250−1261.
(5) Li, N.; Zhao, P.; Astruc, D. Anisotropic Gold Nanoparticles: Synthesis, Properties, Applications, and Toxicity. *Angew. Chem., Int. Ed.* **2014**, *53* (7), 1756−1789.
(6) Link, S.; El-Sayed, M. A. Shape and size dependence of radiative, non-radiative and photothermal properties of gold nanocrystals. *Int. Rev. Phys. Chem.* **2000**, *19* (3), 409−453.
(7) Yang, Y.; Liao, S.; Luo, Z.; Qi, R.; Mac Fhionnlaoich, N.; Stellacci, F.; Guldin, S. Comparative characterisation of non-monodisperse gold nanoparticle populations by X-ray scattering and electron microscopy. *Nanoscale* **2020**, *12* (22), 12007−12013.
(8) Amendola, V.; Meneghetti, M. Size Evaluation of Gold Nanoparticles by UV−vis Spectroscopy. *J. Phys. Chem. C* **2009**, *113* (11), 4277−4285.
(9) McKenzie, L. C.; Haben, P. M.; Kevan, S. D.; Hutchison, J. E. Determining Nanoparticle Size in Real Time by Small-Angle X-ray Scattering in a Microscale Flow System. *J. Phys. Chem. C* **2010**, *114* (50), 22055−22063.
(10) Khlebtsov, B. N.; Khlebtsov, N. G. On the measurement of gold nanoparticle sizes by the dynamic light scattering method. *Colloid J.* **2011**, *73* (1), 118−127.
(11) Mansour, Y.; Battie, Y.; En Naciri, A.; Chaoui, N. Determination of the Size Distribution of Metallic Colloids from Extinction Spectroscopy. *Nanomaterials* **2021**, *11* (11), 2872.
(12) Kálomista, I.; Kéri, A.; Ungor, D.; Csapó, E.; Dékány, I.; Prohaska, T.; Galbács, G. Dimensional characterization of gold nanorods by combining millisecond and microsecond temporal resolution single particle ICP-MS measurements. *Journal of Analytical Atomic Spectrometry* **2017**, *32* (12), 2455−2462.
(13) Liu, J.; Murphy, K. E.; MacCuspie, R. I.; Winchester, M. R. Capabilities of Single Particle Inductively Coupled Plasma Mass Spectrometry for the Size Measurement of Nanoparticles: A Case Study on Gold Nanoparticles. *Anal. Chem.* **2014**, *86* (7), 3405−3414.
(14) Plutschack, M. B.; Pieber, B.; Gilmore, K.; Seeberger, P. H. The Hitchhiker's Guide to Flow Chemistry. *Chem. Rev.* **2017**, *117* (18), 11796−11893.
(15) Haiss, W.; Thanh, N. T. K.; Aveyard, J.; Fernig, D. G. Determination of Size and Concentration of Gold Nanoparticles from UV−Vis Spectra. *Anal. Chem.* **2007**, *79* (11), 4215−4221.
(16) Wang, X.; Cao, Y. Characterizations of absorption, scattering, and transmission of typical nanoparticles and their suspensions. *Journal of Industrial and Engineering Chemistry* **2020**, *82*, 324−332.
(17) Iqbal, M.; Usanase, G.; Oulmi, K.; Aberkane, F.; Bendaikha, T.; Fessi, H.; Zine, N.; Agusti, G.; Errachid, E.-S.; Elaissari, A. Preparation of gold nanoparticles and determination of their particles size via different methods. *Mater. Res. Bull.* **2016**, *79*, 97−104.
(18) Hu, Z. J.; Hou, S.; Ji, Y. L.; Wen, T.; Liu, W. Q.; Zhang, H.; Shi, X. W.; Yan, J.; Wu, X. C. Fast characterization of gold nanorods ensemble by correlating its structure with optical extinction spectral features. *AIP Adv.* **2014**, *4* (11), No. 117137.
(19) Njoki, P. N.; Lim, I. I. S.; Mott, D.; Park, H.-Y.; Khan, B.; Mishra, S.; Sujakumar, R.; Luo, J.; Zhong, C.-J. Size Correlation of Optical and Spectroscopic Properties for Gold Nanoparticles. *J. Phys. Chem. C* **2007**, *111* (40), 14664−14669.
(20) Pinho, B.; Torrente-Murciano, L. Dial-A-Particle: Precise Manufacturing of Plasmonic Nanoparticles Based on Early Growth Information—Redefining Automation for Slow Material Synthesis. *Adv. Energy Mater.* **2021**, *11* (32), No. 2100918.
(21) Tuersun, P.; Zhu, C.; Han, X.; Fang Ren, K.; Yin, Y. Light extinction spectrometry for determining the size distribution and concentration of polydisperse gold nanospheres. *Optik* **2020**, *204*, No. 163676.
(22) Eustis, S.; El-Sayed, M. A. Determination of the aspect ratio statistical distribution of gold nanorods in solution from a theoretical fit of the observed inhomogeneously broadened longitudinal plasmon resonance absorption spectrum. *J. Appl. Phys.* **2006**, *100* (4), No. 044324.
(23) Meza Ramirez, C. A.; Greenop, M.; Ashton, L.; Rehman, I. U. Applications of machine learning in spectroscopy. *Appl. Spectrosc. Rev.* **2021**, *56* (8−10), 733−763.
(24) Tao, H.; Wu, T.; Aldeghi, M.; Wu, T. C.; Aspuru-Guzik, A.; Kumacheva, E. Nanoparticle synthesis assisted by machine learning. *Nature Reviews Materials* **2021**, *6* (8), 701−716.
(25) Tan, E. X.; Chen, Y.; Lee, Y. H.; Leong, Y. X.; Leong, S. X.; Stanley, C. V.; Pun, C. S.; Ling, X. Y. Incorporating plasmonic featurization with machine learning to achieve accurate and bidirectional prediction of nanoparticle size and size distribution. *Nanoscale Horizons* **2022**, *7* (6), 626−633.
(26) Malkiel, I.; Mrejen, M.; Nagler, A.; Arieli, U.; Wolf, L.; Suchowski, H.; Malkiel, I.; Mrejen, M.; Nagler, A.; Arieli, U.; Wolf, L.; Suchowski, H. *Plasmonic nanostructure design and characterization via Deep Learning*; Light: Science & Applications, 2018. *7*(1): p 60.
(27) Luo, J.; Li, X.; Zhang, X.; Guo, J.; Liu, W.; Lai, Y.; Zhan, Y.; Huang, M. Deep-learning-enabled inverse engineering of multi-wavelength invisibility-to-superscattering switching with phase-change materials. *Opt. Express* **2021**, *29* (7), 10527−10537.
(28) Karlik, B.; Yilmaz, M. F.; Ozdemir, M.; Yavuz, C. T.; Danisman, Y. A Hybrid Machine Learning Model to Study UV-Vis Spectra of Gold Nanospheres. *Plasmonics* **2021**, *16* (1), 147−155.
(29) He, J.; He, C.; Zheng, C.; Wang, Q.; Ye, J. Plasmonic nanoparticle simulations and inverse design using machine learning. *Nanoscale* **2019**, *11* (37), 17444−17459.
(30) Peurifoy, J.; Shen, Y.; Jing, L.; Yang, Y.; Cano-Renteria, F.; DeLacy, B. G.; Joannopoulos, J. D.; Tegmark, M.; Soljačić, M. Nanophotonic particle simulation and inverse design using artificial neural networks. Science. *Advances* **2018**, *4* (6), No. eaar4206.
(31) So, S.; Mun, J.; Rho, J. Simultaneous Inverse Design of Materials and Structures via Deep Learning: Demonstration of Dipole Resonance Engineering Using Core−Shell Nanoparticles. *ACS Appl. Mater. Interfaces* **2019**, *11* (27), 24264−24268.
(32) Shiratori, K.; Bishop, L. D. C.; Ostovar, B.; Baiyasi, R.; Cai, Y.-Y.; Rossky, P. J.; Landes, C. F.; Link, S. Machine-Learned Decision Trees for Predicting Gold Nanorod Sizes from Spectra. *J. Phys. Chem. C* **2021**, *125* (35), 19353−19361.
(33) Glaubitz, C.; Bazzoni, A.; Ackermann-Hirschi, L.; Baraldi, L.; Haeffner, M.; Fortunatus, R.; Rothen-Rutishauser, B.; Balog, S.; Petri-Fink, A. Leveraging Machine Learning for Size and Shape Analysis of Nanoparticles: A Shortcut to Electron Microscopy. *J. Phys. Chem. C* **2024**, *128* (1), 421−427.
(34) LeCun, Y.; Bengio, Y.; Hinton, G. Deep learning. *Nature* **2015**, *521* (7553), 436−444.
(35) Oskooi, A. F.; Roundy, D.; Ibanescu, M.; Bermel, P.; Joannopoulos, J. D.; Johnson, S. G. Meep: A flexible free-software package for electromagnetic simulations by the FDTD method. *Comput. Phys. Commun.* **2010**, *181* (3), 687−702.
(36) Girard, C. Near fields in nanostructures. *Rep. Prog. Phys.* **2005**, *68* (8), 1883.
(37) Joannopoulos, J. D. *Photonic crystals: molding the flow of light*; 2nd ed. Princeton University Press, 2008
(38) Chollet, F. *Keras. Version 2.5.0* [Internet] 2015 [Accessed 6 January 2023]; Available from: https://keras.io.
(39) Pan, S. J.; Yang, Q. A Survey on Transfer Learning. *IEEE Transactions on Knowledge and Data Engineering* **2010**, *22* (10), 1345−1359.

https://doi.org/10.1021/acs.jpcc.4c02971
J. Phys. Chem. C XXXX, XXX, XXX−XXX

Supporting Information

Machine Learning-Based Interpretation of Optical Properties of Colloidal Gold with Convolutional Neural Networks

Frida Bilén[1], Pernilla Ekborg-Tanner[2], Antoine Balzano[1], Michaël Ughetto[3], Robson Rosa da Silva[1, 4], Hannes Schomaker[1, 5], Paul Erhart[2], Kasper Moth-Poulsen[1, 6, 7, 8], Romain Bordes[1*].

[1] Department of Chemistry and Chemical Engineering, Chalmers University of Technology, Gothenburg, 412 58, Sweden
[2] Department of Physics, Chalmers University of Technology, Gothenburg, 412 96, Sweden
[3] BIKG, AI Strategy & Innovation, R&D IT, AstraZeneca AB, Mölndal, 431 83, Sweden
[4] NanoScientifica Scandinavia AB, Gothenburg, 412 96, Sweden
[5] AutoSyn AB, Hisings Backa, 422 57, Sweden
[6] Department of Chemical Engineering, Universitat Politècnica de Catalunya, Barcelona, 08019, Spain.
[7] Catalan Institution for Research & Advanced Studies, ICREA, Barcelona, 08010, Spain.
[8] Institute of Materials Science of Barcelona, ICMAB-CSIC, Barcelona, 08193, Spain.

*** Corresponding author:**

E-mail address: bordes@chalmers.se

1 SIMULATED SINGLE PARTICLE SPECTRA

Single particle spectra were simulated with the finite-difference time-domain (FDTD) method, and the simulated spectra are presented in Figure S1 for the spherical particles and Figure S2 for the rod-shaped particles. As can be seen in the figures, the spectra show wavy disturbances at larger wavelengths, and preprocessing was therefore made where the wavelengths were limited to 400-800 nm for the sphere spectra and 400-1000 nm for the rod spectra. The reason for including longer wavelengths for the rods is that more information was present at longer wavelengths for the rods which was desired to be included in the spectra.

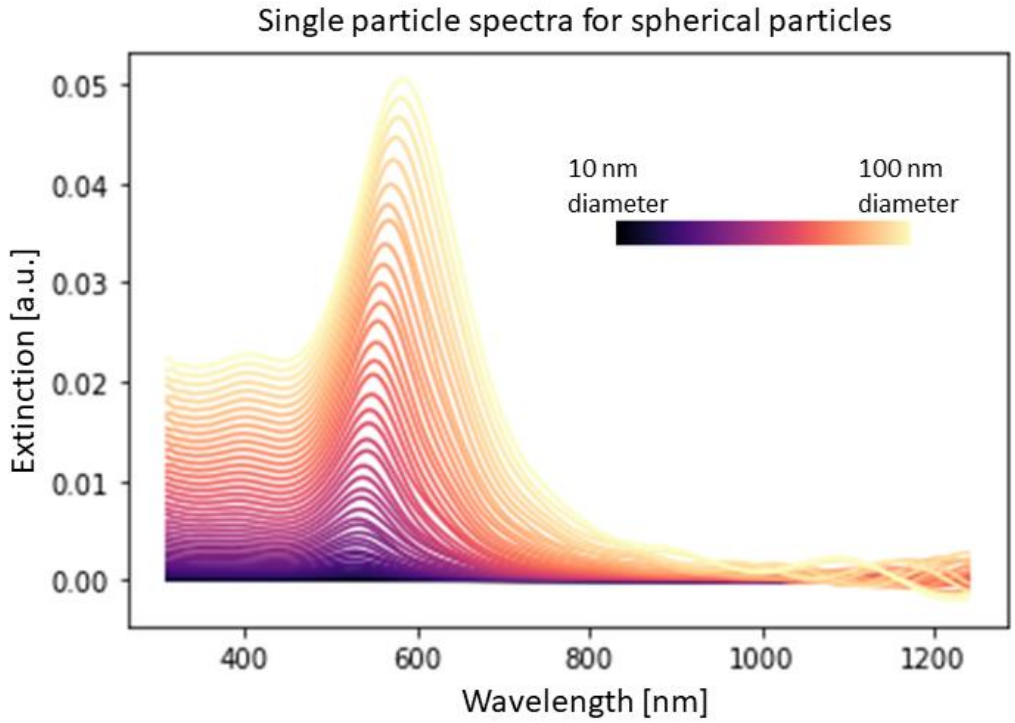

Figure S1. The single particle spectra simulated with the FDTD method for spherical gold nanoparticles.

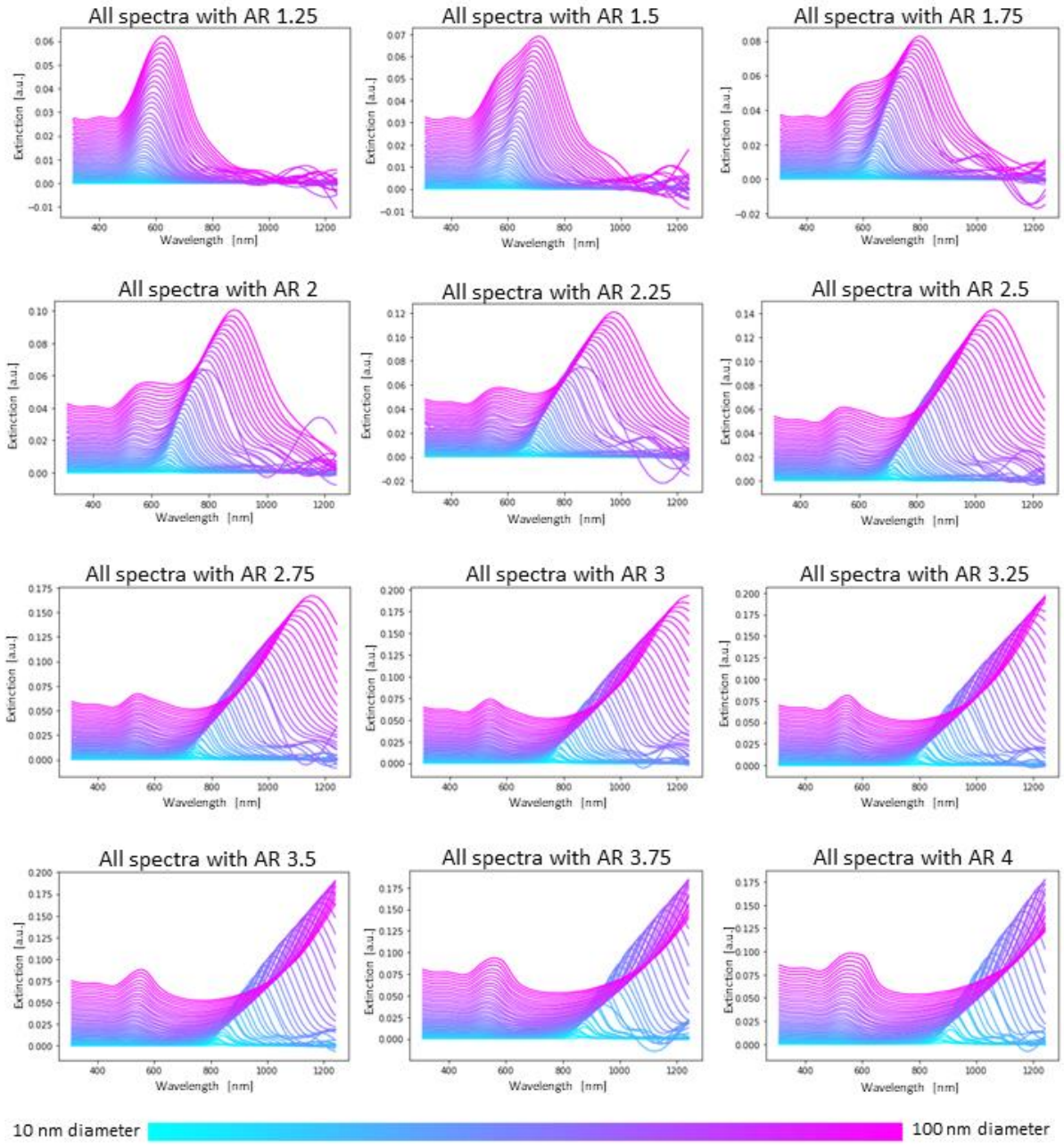

Figure S2. All single particle spectra for rod shaped particles, as simulated by the FDTD method, sorted by their aspect ratio.

As can be seen in Figure S2, some single particle spectra for rod-shaped particles diverge from the trend of the rest of the spectra. This behavior can be attributed to numerical instabilities inherent to FDTD simulations, especially when the wavelength approaches the cell size. Since the majority of the simulations resulted in smooth trends (indicating stable simulations), the outliers were replaced by interpolations based on neighboring spectra, rather than replacing them with computationally more expensive simulations. In Figure S3 one example of the preprocessing step is presented, where the diverging spectra have been replaced with interpolations (marked in green) and the wavelength range has been limited to 400-1000 nm.

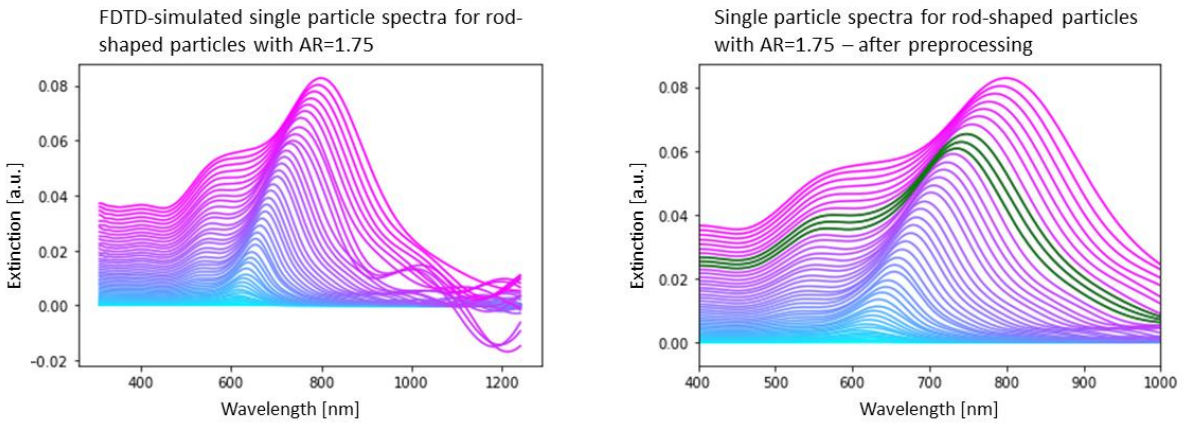

Figure S3. An example of the preprocessing done for the single particle spectra of rod-shaped particles. To the left are the spectra for particles with AR=1.75, as they were simulated by the FDTD method. To the right are the spectra after preprocessing, where the wavelength range has been limited and a few spectra have been replaced by interpolations (marked in green) based on other spectra with the same aspect ratio.

2 MODEL ARCHITECTURE

2.1 SPHERE MODEL ARCHITECTURE

Model layers:

1. Conv2D: filters = 8, kernel size = (1,150), strides = (1,1), activation = ReLU, padding = “same", input shape = (1, 206, 1)
2. Conv2D: filters = 16, kernel size = (1,120), strides = (1,1), activation = ReLU, padding = “same"
3. MaxPooling2D: pool size = (1,2), strides = (1,2)
4. Conv2D: filters = 32, kernel size = (1,80), strides = (1,2), activation = ReLU, padding = “same"
5. Conv2D: filters = 64, kernel size = (1,40), strides = (1,2), activation = ReLU, padding = “same"
6. MaxPooling2D: pool size = (1,2), strides = (1,2)
7. Flatten
8. Dense: 30 units, activation = ReLU
9. Dense: 2 units, no activation function

Compilation: Loss = Mean squared error, optimizer = Adam with default learning rate (0.001), metrics = Mean squared error

Model fitting: 600 epochs with ModelCheckpoint callback. Validation split = 0.3, batch size = 100.

2.2 ROD MODEL ARCHITECTURE

Model layers:

1. Conv2D: filters = 16, kernel size = (1,50), strides = (1,1), activation = ReLU, padding = “same", input shape = (1, 248, 1)
2. Conv2D: filters = 32, kernel size = (1,40), strides = (1,1), activation = ReLU, padding = “same"
3. MaxPooling2D: pool size = (1,2), strides = (1,2)
4. Conv2D: filters = 64, kernel size = (1,20), strides = (1,2), activation = ReLU, padding = “same"
5. Conv2D: filters = 128, kernel size = (1,10), strides = (1,2), activation = ReLU, padding = “same"
6. MaxPooling2D: pool size = (1,2), strides = (1,2)
7. Flatten
8. Dense: 60 units, activation = ReLU
9. Dense: 4 units, no activation function

Compilation: Loss = Mean squared error, optimizer = Adam with default learning rate (0.001), metrics = Mean squared error

Model fitting: 600 epochs with ModelCheckpoint callback. Validation split = 0.3, batch size = 100.

3 EXPERIMENTAL SPECTRA FOR COMPARISONS

3.1 NOISE ESTIMATION

As a comparison between experimental data and the simulated data with added noise, the noise level was estimated for two experimental spectra of different gold nanosphere dispersions. The noise level was estimated by denoising the spectra by applying a Savitzky-Golay filter with a window length of 15 and polynomial order of 2 with the SciPy signal processing function savgol_filter in Python. The standard deviation of the difference between the noisy spectrum and the denoised version was determined as the noise level, in a similar fashion to how the noise level was decided for the simulated spectra. The noise levels for the two experimentally recorded spectra were 0.001 and 0.003 respectively, see Figure S4.

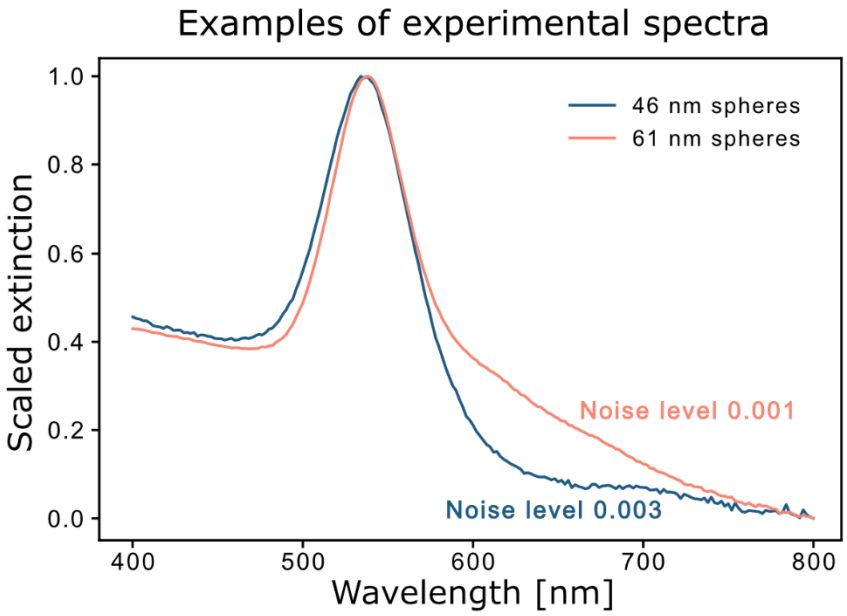

Figure S4. Two examples of experimental UV-Vis spectra for spherical gold nanoparticles, and the estimated noise level expressed as the standard deviation of the datapoints in comparison to a denoised spectrum version.